PROPELLER THRUST ANALYSIS USING PRANDTL'S LIFTING LINE THEORY, A COMPARISON BETWEEN THE EXPERIMENTAL THRUST AND THE THRUST PREDICTED BY PRANDTL'S LIFTING LINE THEORY

by

Steven R. Kesler

A thesis submitted to the faculty of
The University of Utah
in partial fulfillment of the requirements for the degree of

Master of Science

Department of Mechanical Engineering

The University of Utah

August 2014

Copyright © Steven R. Kesler 2014

All Rights Reserved

The University of Utah Graduate School

STATEMENT OF THESIS APPROVAL

The thesis of **Steven R. Kesler**

has been approved by the following supervisory committee members:

Kuan Chen	, Chair	**05/05/2014** Date Approved
Sanford G. Meek	, Member	**05/05/2014** Date Approved
Ken Monson	, Member	**04/25/2014** Date Approved

and by **Tim Ameel** , Chair/Dean of

the Department/College/School of **Mechanical Engineering**

and by David B. Kieda, Dean of The Graduate School.

ABSTRACT

The lifting line theory was first developed by Prandtl and was used primarily on analysis of airplane wings. Though the theory is about one hundred years old, it is still used in the initial calculations to find the lift of a wing.

The question that guided this thesis was, "How close does Prandtl's lifting line theory predict the thrust of a propeller?" In order to answer this question, an experiment was designed that measured the thrust of a propeller for different speeds. The measured thrust was compared to what the theory predicted. In order to do this experiment and analysis, a propeller needed to be used. A walnut wood ultralight propeller was chosen that had a 1.30 meter (51 inches) length from tip to tip.

In this thesis, Prandtl's lifting line theory was modified to account for the different incoming velocity depending on the radial position of the airfoil. A modified equation was used to reflect these differences. A working code was developed based on this modified equation.

A testing rig was built that allowed the propeller to be rotated at high speeds while measuring the thrust. During testing, the rotational speed of the propeller ranged from 13-43 rotations per second. The thrust from the propeller was measured at different speeds and ranged from 16-33 Newton's. The test data were then compared to the theoretical results obtained from the lifting line code. A plot in Chapter 5 (the results section) shows the theoretical vs. actual thrust for different rotational speeds.

The theory over predicted the actual thrust of the propeller. Depending on the rotational speed, the error was: at low speeds 36%, at low to moderate speeds 84%, and at high speeds the error increased to 195%. Different reasons for these errors are discussed.

This thesis is dedicated to my wife, who has supported me throughout this process and to my parents, who encouraged me to pursue worthwhile goals.

TABLE OF CONTENTS

LIST OF FIGURES

NOMENCLATURE

V or V_∞	Incoming velocity	(m/s)
$V_\infty(y_0)$	Incoming velocity at different spanwise locations	(m/s)
$V_\infty(\emptyset_0)$	Incoming velocity at different spanwise locations in terms of the transform variable	(m/s)
v	Induced velocity	(m/s)
ρ	Density	(kg/m^3)
A	Rotor disk area	(m^3)
P	Power loss	(Watts)
T	Thrust	(Newton's)
$L_{perSpan}$	Lift per span	(Newton's/meters)
L_{total}	Total lift	(Newton's)
Γ	Circulation	(m^2/sec)
$\Gamma(y_0)$	Circulation at different spanwise locations	(m^2/sec)
$\propto_{L=0}$	Zero lift angle of attack	(radians)
$\propto_{L=0}(y_0)$	Zero lift angle of attack at different spanwise locations	(radians)
$\propto(y_0)$	Angle of attack at different spanwise locations	(radians)
$\propto(\emptyset_0)$	Angle of attack at different spanwise locations in terms of the transform variable	(radians)
x	Coordinate direction in the same direction as the incoming flow	
y or y_0	Coordinate direction in the spanwise direction of the propeller blade	

z	Coordinate direction perpendicular to both the incoming flow and spanwise direction	
$\emptyset$	Transform variable	
c	Chord length	(meters)
$c(y_0)$	Chord length at different spanwise locations	(meters)
$c(\emptyset_0)$	Chord length at different spanwise locations in terms of the transform variable	(meters)
B	Length of the propeller blade	(meters)
A_n	Coefficients used to generate the Fourier Series approximation of the circulation	
$Thrust_{actual}$	The thrust measured by the testing rig	(Newton's)
$Thrust_{theretical}$	The thrust calculated by the computer code	(Newton's)
Re	Renolds number	
μ	Fluid viscosity	(kg/(sec*m))

ACKNOWLEDGMENTS

Foremost, I would like to express my appreciation to my advisor, Professor Kuan K Chen. I have learned a great deal about aerodynamics as I have sat in his lectures and as we have talked one on one about this thesis.

I am also very grateful for Sanford G. Meek and Ken Monson for their encouragement and feedback.

CHAPTER 1

INTRODUCTION

Prandtl's lifting line theory, (Anderson, 2007) though old, is good for doing a quick analysis. It gives a closed-form solution so that key parameters for the design can be found. Though Prandtl's lifting line theory has been used in finite wings, it has not been used to analyze propellers. Other tools exist to analyze propellers, but a lot of them do not have closed-form solutions. There is a common theory called the Blade Element Theory that is used to analyze propellers. The Blade Element Theory gives a closed-form solution, but this theory requires a fudge factor in order to accommodate for invalid assumptions in the development of the theory. One big advantage of using the lifting line theory was that the closed-form solution did not require fudge factors and an actual closed-form solution was found. It was not as computationally intense as a Finite Element Analysis model (FEA) and it did not require as much setup as an FEA. Some of the limitations to Prandtl's lifting line theory came from the assumptions that were used to develop the equation. The flow is assumed to be inviscid and incompressible. The inviscid flow assumption is a good approximation because at the higher speeds and the low viscosity, most of the forces come from the pressure distribution on the airfoil, and only a small portion will come from the skin friction.

Assuming that the fluid is incompressible is valid as long as the propeller is not close to the speed of sound. The part of the propeller that will have the highest velocity is

the propeller tip. As long as the tip velocity is one third the speed of sound, it can be safely assumed that the flow will be incompressible.

Another assumption that was made in Prandtl's lifting line theory was that the incoming velocity would be smooth. This is never the case in the context of propeller analysis. Due to the complex disturbance caused by the preceding blade, the incoming velocity is hard to model. While this was an invalid assumption, a smooth incoming flow was used because it is almost impossible to model the complex flow of what actually happens. This will be further discussed in the literature review.

The question that guided this thesis was "How close does Prandtl's lifting line theory predict the thrust of a propeller?" In order to answer this question, this thesis had two main parts. The first was developing a modification to Prandtl's lifting line equation for studying propellers. The second part of this thesis was to perform an experiment that measured a few key parameters. The results from these two parts were then compared.

The velocity terms in the original Prandtl's lifting line equation had to be modified in order to use them for propellers. The original Prandtl's lifting line equation assumed a constant incoming air velocity in the context of airplane analysis. This is not the case with propeller analysis. The tip of the propeller moves faster than any other part of the propeller, and the hub moves slower than any other part of the propeller. Prandtl's lifting line theory had to be altered in order to reflect this difference and is shown in an integro differential equation. In order to solve the integro differential equation, a Fourier Series was used. This approach was similar to what Prandtl did except there were velocity terms in the equation that were different, and the boundary conditions were different. A computer code was developed to solve the integro differential equation. The

code used inputs of the propeller geometry and the rotational speed, and the output was the thrust of the propeller.

The second part of this thesis consisted of designing and running tests that measured the thrust of a propeller. A propeller was also designed and built. The test rig frame was built out of multiple 2" diameter pipes. Three wheels where connected to the frame. The test rig was powered by a 40 horse power engine. The drive train consisted of a centrifugal clutch. Two sensors were also designed and built. The first sensor was a speed sensor and the second sensor was a thrust sensor. These sensors were connected to a Data Acquisition System (DAQ) system, which was connected to a laptop. When the test was performed, each wheel on the test rig was placed on a smooth surface. The surface allowed the rig to roll back and forth with very little friction. The thrust sensor was anchored to the ground on one end and on the other end was fastened to the test rig. By using this setup, the only load path from the thrust of the propeller was through the thrust sensor. When the tests were performed, the thrust from the propeller applied a force to the thrust sensor. This would make the springs in the thrust sensor deflect until the forces were equalized. Before any tests were run, both the speed and thrust sensors were calibrated. During the tests, both the thrust and speed were measured. A plot was constructed from these data to show the thrust of the propeller at different speeds.

The same speeds from the experiment were analyzed in the software that was developed. With both the experimental and theoretical results, the data were then compared to each other. The results found that the theory over predicted the actual thrust of the propeller. Depending on the rotational speed, the error was between 36% to 84% for low to moderate speeds, but at high speeds, the error increased to 195%. The reasons

for these errors are in part due to the assumptions that were made in the development of Prandtl's lifting line theory.

CHAPTER 2

LITERATURE REVIEW

This chapter describes literature relevant to the research purposes of this thesis. I first review previous scholarly literature on propeller design and analysis. This review will include a discussion of different propeller theories, their uses, and limitations. The final section of the literature review discusses the theoretical approach for the study, Prandtl's lifting line theory.

Propellers are used in a wide range of machinery. They are used in boats, airplanes, windmills, and ventilation systems as well as many other types of machinery. Propellers have been studied from many approaches to optimize the efficiency of the device in which they are used. Some approaches to studying propellers include the Momentum Theory, the Blade Element Theory, the Vortex Theory, and Computational Fluid Dynamics (Johnson, 1994). These theoretical concepts will be discussed in the following sections.

1.1 Momentum Theory

In fluid dynamics, momentum theory (Johnson, 1994) describes a mathematical model for propellers. One of the earliest methods used for analyzing propellers was this theory. Johnson stated that "The purpose of momentum theory is to find the induced velocity and power for a given thrust" (Johnson, 1994) and "this method is surpassed in accuracy by more modern theory but is still used to give a first approximation" (pp. 29-

30). The way the momentum theory finds the induced velocity and power for a given thrust is by using conservation of momentum, energy, and mass. Stepniewski and Keys (1984) said, "the momentum approach may provide a clarity of the overall picture that could be lacking when more complicated theories are applied" (p. 89).

One of the basic concepts that can be understood from momentum theory is the slipstream of a propeller. When an airplane propeller produces thrust, it forces air behind the aircraft and produces a slipstream. Rwigema (2010) found that the slipstream **"**may rudimentarily be considered as a cylindrical tube of spiraling air propagating rearward over the fuselage and wings – having detrimental and beneficial effects. Flow within the slipstream is faster than free-stream flow resulting in increased drag over the parts exposed to its trajectory" (Rwigema, 2010, p. 2). The slipstream is related to the size of the propeller and it helps design engineers understand the dynamics of the air. This is important to understand in the design process of the propeller because it will affect other measurable factors, or parameters, of the propeller.

In momentum theory, the propeller is analyzed as an actuator disk. It is infinitely thin. The velocity does not change across the disk, but the pressure does. Figure 1 shows the slipstream of a propeller as well as other parameters.

The momentum theory uses the following equations (Johnson, 1994, p. 33) which describe the induced velocity (v) and power loss (P). The different parameters are 'ρ' for the density, 'A' for the area of the propeller disk, and the parameters as shown in Figure 1.

$$\mathbf{v} = -\frac{\boldsymbol{V}}{\mathbf{2}} + \sqrt{\left(\frac{\boldsymbol{V}}{\mathbf{2}}\right)^{\mathbf{2}} + \left(\frac{\boldsymbol{T}}{\mathbf{2}*\boldsymbol{\rho}*\boldsymbol{A}}\right)} \quad \textbf{(1)}$$

$$\boldsymbol{P} = \boldsymbol{T}(\boldsymbol{V} + \mathbf{v}) \quad \textbf{(2)}$$

Referring to the momentum theory, Stepniewski and Keys (1984) asserted that

> The presently discussed theory [momentum theory] encounters serious limitations in providing guidance for rotor design, as it singles out disc loading as the only important parameter. Consequently, it does not provide any insight into such rotor characteristics as ratio of the blade area to the disc area, blade airfoil characteristics, tip speed values with all the associated phenomena of compressibility, etc. … the simple momentum approach did not provide a physical concept that could explain the non uniformities of downwash velocities or the presence of tip losses. (p. 89)

As discussed above, the uniform disk loading is an assumption made by momentum theory. In reality, the propeller will be loaded closer to the middle of the blade and less near the tips and the hubs. This will make the slipstream less uniform then what is assumed by momentum theory. Though the momentum theory is good to understand the basic fluid dynamics from propellers, other theories need to be used when a more rigorous study is undertaken in propeller analysis and design.

1.2 Blade Element Theory

A widely used theory in propeller design and analysis is the Blade Element Theory (Rwigema, 2010). The Blade Element Theory is "a model which will permit one to determine… aerodynamic forces and moments acting on various segments of the blade" and this can be done by "imagining that the blade is composed of aerodynamically independent, chord wise-oriented, narrow strips or elements" (Stepniewski and Keys, 1984, 93). This is a powerful theory because only the two-dimensional characteristics of an airfoil needs to be known in order to determine the forces of a three-dimensional flow.

Though the analysis is straightforward, there are a lot of assumptions and associated errors. "There is no interaction between the analyses of each blade element, and the forces exerted on the blade elements by the flow stream are determined solely by

the two-dimensional lift and drag characteristics of the blade element airfoil shape and orientation relative to the incoming flow"(Rwigema, 2010, p. 3). This assumption is valid at most places on the propeller, but one place that this assumption grossly over predicts the lift is near the propeller tips. The air underneath the airfoil goes around the tip of the propeller toward the top of the airfoil. This has the effect of decreasing the lift at the tip of the blade. The fluid moving from the bottom to the top of the wing is called wing tip vortices. Rwigema (2010) explains, "These tip vortices create multiple helical structures in the wake and play a major role in the induced velocity distribution along the propeller. To compensate for this deficiency in Blade Element Theory, a tip-loss (or correction) factor, F, originally developed by Prandtl is used" (Rwigema, 2010, p. 4). The wing tip vortices create a component of velocity perpendicular to the flow. This induced velocity decreases the effective angle of attack of the airfoil at different spanwise locations; see Figure 2. This will be manifested by the steady decrease of lift nearing the tips until the lift goes to zero at the very tips. Figure 3 shows the lift along the propeller predicted by the Blade Element Theory, and the lift that is expected because of wing tip losses.

Referencing Figure 2, the V_inf is the approach velocity of the airstream, and V_ind is the induced velocity from the wing tip vortices. The vector sum of these two velocity components is V_sum. Because of the induced velocity (V_ind) created from the wing tip vortices, the geometric angle of attack (A) is not what determines the lift of the airfoil. The lift is determined by the effective angle of attack (B). The induced velocity along the propeller blade is small near the middle, and increases nearer the wing tips.

Blade Element Theory is still widely used in the analysis of propellers. Rashahmadi (2011) said, "Blade Element Theory remains popular due to their low costs and realizibility…" (p. 1582). Though there are errors in using this theory, one of the biggest advantages is the ease of the theory's application. Results that are more accurate can be calculated using the correction factors described above, but these are not exact and there will still be errors. For more accurate analysis, or when the geometry does not lend itself to Blade Element Theory, other theories can be used. Another theory that is commonly used is vortex theory.

1.3 Vortex Theory

Another theory through which propeller can be studied is through the vortex theory. The vortex theory works by accounting for the lift of an object by looking at the circulation of a fluid instead of the pressure on the object. This concept is explained by the Kutta-Joukowski Theorem (Johnson, 1994, p. 262), which is mathematically shown below.

$$\boldsymbol{L_{perSpan} = \rho * V * \Gamma} \quad \textbf{(3)}$$

1.4 Thin Airfoil Theory

One application of the vortex theory is the thin airfoil theory. This theory is for 2D flow only. Anderson (2007) explains how the "thin airfoil theory provides a means to predict the angle of zero lift" (p. 333) . The zero lift angle of attack is the angle of attack that the airfoil is at when no lift is generated. In addition, thin airfoil theory predicts the slope of the lift vs. angle curve to be 2*pi. The equation is developed by treating the

mean camber of the airfoil as a streamline in the flow (Anderson, 2007). Equation 4 shows the equation derived by the thin airfoil theory, that equates the zero lift angle of attack to the shape of the camber line. Equation 5 is a transform between the variable x and ∅, z is the heigth of the camber of the airfoil in the x direction and c is the chord length.

$$\propto_{L=0} = -\frac{1}{pi} * \int_0^{pi} \frac{dz}{dx} * (\cos \emptyset - 1)\, d\emptyset \quad \textbf{(4)}$$

$$x = \left(\frac{c}{2}\right) * (cos\emptyset - 1) \quad \textbf{(5)}$$

The vortex theory can be used to set up numerical solutions. Johnson (1994) said, "The modern variant of the vortex theory is a numerical solution for the rotor induced velocity, loads, and performance that uses a detailed model of the vortex wake, including a representation of the discrete tip vortices and frequently even the distorted wake geometry. Such an analysis is only practical using high-speed digital computers" (p. 88). The vortex theory is a powerful theory that can be used in numerical computations and in other simpler calculations like the thin airfoil theory. The vortex lattice method is a numerical solution that can be used for three-dimensional flow.

Other current numerical solutions exist beyond the vortex lattice method. The finite volume method used by most computational fluid dynamic code in solving the Navier-Stokes equation is a powerful technology and is used extensively in the aerospace industry.

Kerwin (2001) points out some shortcomings of propeller analysis and of numerical solutions in general. Talking about the flow field around the propeller, he said, "Unlike a purely potential flow, the vorticity in this flow field interacts with itself as it is accelerated by the action of the propeller. This means that the total velocity at a point

near the propeller is not simply the linear superposition of the inflow (in the absence of the propeller) and the velocity induced by the propeller, but includes an additional interactive component" (p. 134). The momentum theory, Blade Element Theory, and many numerical simulations do not take into account the disturbance of the flow going into the propeller blade caused by the wake of the previous propeller blade. Kerwin continues, "A full numerical simulation of the combined flow problem requires massive computational resources, and the validity of the outcome is limited by present empirical modeling of turbulence. It is therefore a practical necessity to employ a simpler flow model for most propeller design and analysis applications" (p. 134).

Prandtl's lifting line theory is a subset of the vortex theory. This is a simple theory that has a closed-form solution. It is similar to Blade Element Theory except this theory takes into account the wing tip vortices.

1.5 Prandtl's Lifting Line Theory

Prandtl's lifting line theory is a method used to describe the circulation at different spanwise locations of the wing. In this thesis, it has been applied to a propeller. From the circulation, the lift at the different sections of the propeller wing were calculated, by using the Kutta-Joukowski Theorem (Johnson, 1994). This theorem is explained by Equation 3.

The lift for a cross section of a finite wing was different than the lift of the same cross section for an infinitely long wing. The reason for this was because the fluid not only moved in a two-dimensional motion in a finite wing, but also had a velocity component that traveled towards and away from the tip of the wing. The air traveled from

the bottom of the wing towards the tip and from the tip to the top of the wing. This created an induced velocity on the air. The overall effect was the angle of attack of each cross section was less.

The classical case of a lifting line theory was developed by Prandtl (Johnson, 1994). The theory and equation that he developed bears his name. The principle used in developing this theory is that multiple line segments have circulation around them, and by using superposition, these line segments are placed along the wing. This is done to simulate the circulation over the wing. The circulation had a different value depending on the spanwise location of the wing. This theory found the circulation distribution over a finite wing (Anderson 2007). The fundamental equation of Prandtl's lifting line is shown below, where $\Gamma(y_0)$ is the only unknown.

$$\propto (\boldsymbol{y_0}) = \frac{\boldsymbol{\Gamma(y_0)}}{\mathbf{pi} * \boldsymbol{V_\infty} * \mathbf{c}(\boldsymbol{y_0})} + \propto_{\boldsymbol{L=0}} (\boldsymbol{y_0}) + \frac{\mathbf{1}}{\mathbf{4} * \mathbf{pi} * \boldsymbol{V_\infty}} * \int_{-\frac{\boldsymbol{b}}{\mathbf{2}}}^{\frac{\boldsymbol{b}}{\mathbf{2}}} \left(\frac{\boldsymbol{d\Gamma}}{\mathbf{dy}}\right) / (\boldsymbol{y_0} - \boldsymbol{y}) * \boldsymbol{dy} \quad \textbf{(6)}$$

These parameters described how the geometric angle of attack ($\propto (y_0)$) is equaled to the effective angle of attack ($\frac{\Gamma(y_0)}{\mathrm{pi} * V_\infty * \mathrm{c}(y_0)} + \propto_{L=0} (y_0)$) plus the induced angle of attack ($\frac{1}{4 * \mathrm{pi} * V_\infty} * \int_{-\frac{b}{2}}^{\frac{b}{2}} \left(\frac{d\Gamma}{\mathrm{dy}}\right) / (y_0 - y) * dy$) at every spanwise location. To solve this integro differential equation, the boundary conditions needed to be known. For propellers, Kerwin (2001) explains that the "circulation goes to zero at the hub and the tips" (p. 181).

"The lifting line theory by itself does not provide any way of determining the lift generated by a particular airfoil shape…" (Kerwin, 2001, p. 115) but needed to be used in conjunction with other theories. The zero lift angle of attack term $\propto_{L=0} (y_0)$ in this equation was found by using the thin airfoil theory.

Prandtl's classical lifting line theory works well for wings that are long and narrow. However, for other types of wings like delta wings or swept wings, the classical lifting line theory is inappropriate (Johnson, 1994) . Another limitation to this theory is it assumes inviscid flow. Another assumption of this theory is that no flow separation occurs. When the angle of attack increases beyond the stall angle, there will be flow separation, but this theory does not predict that.

The lifting line theory is similar to Blade Element Theory, but it has fewer assumptions and it is more accurate. Just like Blade Element Theory, the lifting line theory requires a knowledge of the two-dimensional characteristics of the blade at multiple locations. This theory is still used today for preliminary calculations of finite wings, even though it was developed during the years of 1911-1918 (Johnson, 1994).

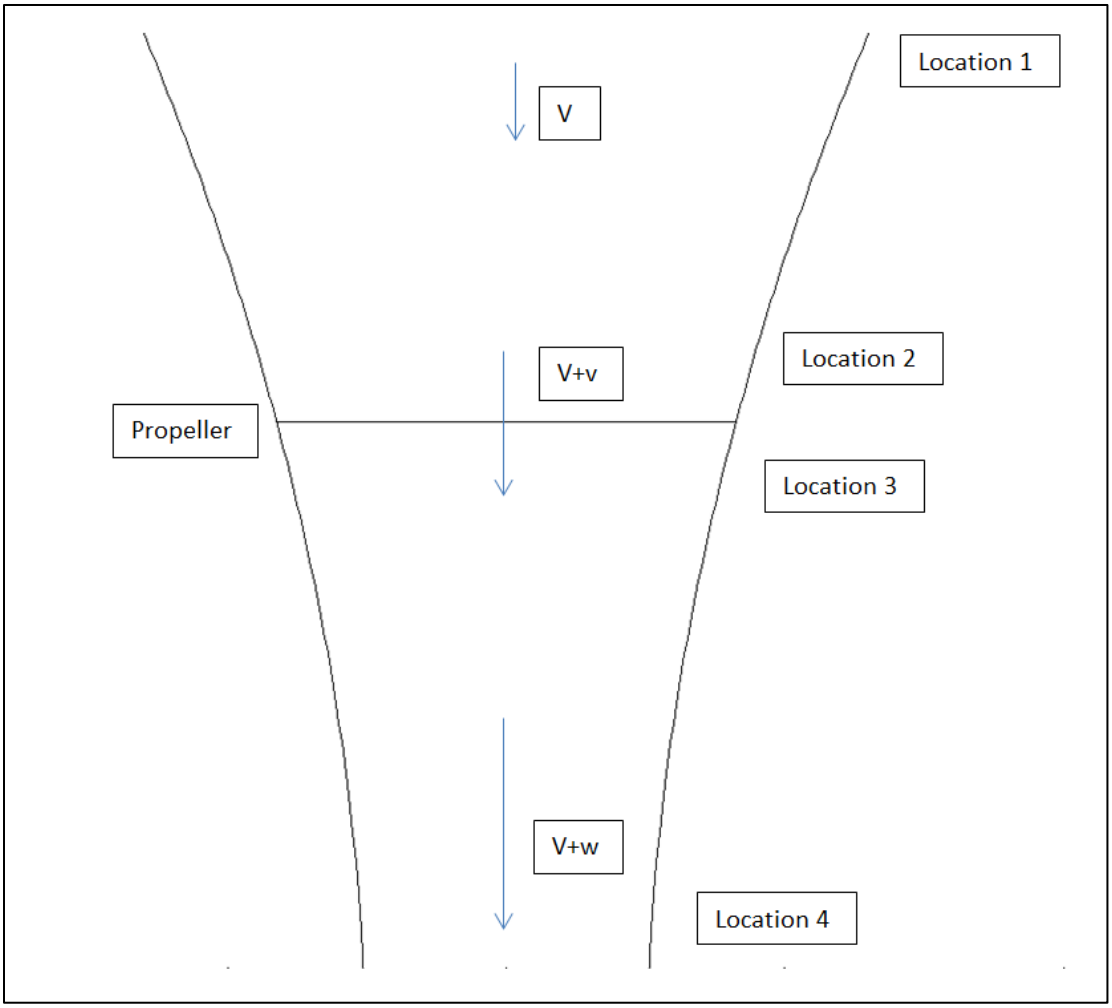

Figure 1: Slipstream of a propeller modeled by the momentum theory

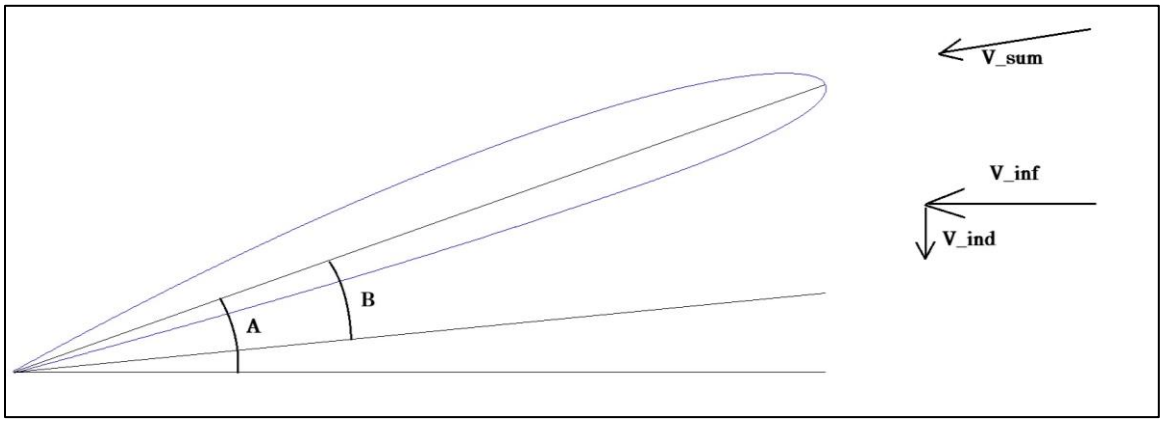

Figure 2: Angle of attack of an airfoil

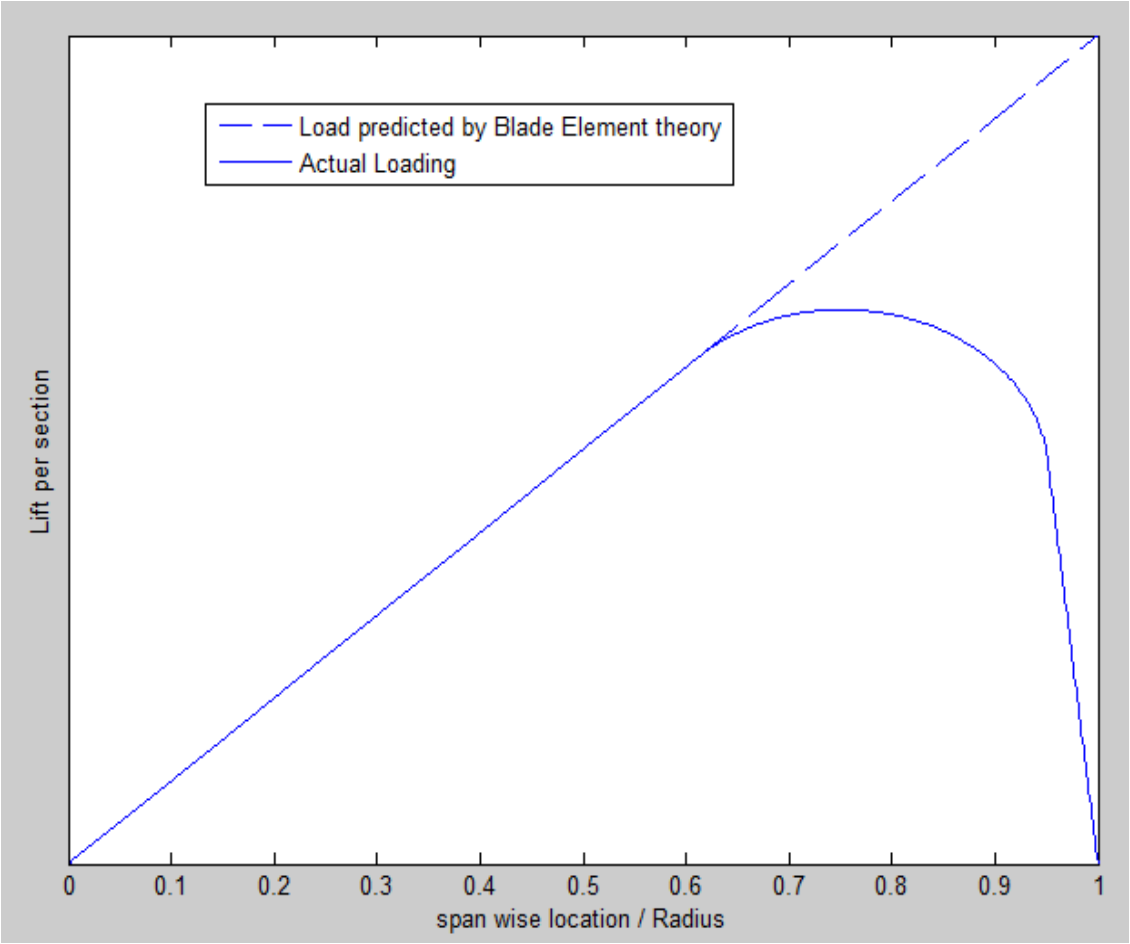

Figure 3: Loading on a propeller for both the actual and the Blade Element Theory

CHAPTER 3

LIFTING LINE THEORY AND CODE DEVELOPMENT

Prandtl's lifting line theory was used to find the overall thrust of a propeller in this thesis. In order to use this lifting line theory, the geometric angle of attack ($\propto$) and the zero lift angle of attack ($\propto_{L=0}$) at different spanwise locations needed to be identified. The approach velocity (V_∞) of the air, chord length (c) and diameter of the propeller (b) also needed to be known. Equation 7 shows the lifting line equation.

$$\propto (y_0) = \frac{\Gamma(y_0)}{\mathrm{pi} * V_\infty * \mathrm{c}(y_0)} + \propto_{L=0} (y_0) + \frac{1}{4 * \mathrm{pi} * V_\infty} * \int_{-\frac{b}{2}}^{\frac{b}{2}} \left(\frac{d\Gamma}{\mathrm{dy}}\right) / (y_0 - y) * dy \quad (7)$$

This equation is the fundamental equation of Prandtl's lifting line theory. By itself, it does not provide a way to determine the lift generated by a particular geometric shape as explained by Kerwin (2001). This equation needed to be combined with other theories in order to determine the thrust generated. The $\propto_{L=0} (y_0)$ term in this equation was found by the thin airfoil theory, and the geometric angle of attack terms ($\propto (y_0)$) were measured. The following section explains how these parameters were found.

2.1 Propeller Geometry

Once the camber of the propeller at multiple spanwise locations was found, the geometric angle of attack and the zero lift angle of attack were identified.

In order to find the camber of the propeller at different spanwise locations, both the top and the bottom surfaces of the propeller were measured. An apparatus was created to measure the top and bottom surface of the propeller at different spanwise locations. The apparatus included an arm that was able to swing around the propeller hub and a caliper that was used to measure the height of the propeller. See Figure 4 for a picture of the measuring apparatus.

The propeller surface was measured at five different spanwise locations. At each spanwise location, the surface of the propeller blade was measured twenty times from the leading edge to the trailing edge on both the top and the bottom of the propeller. An illustration of where the propeller was measured is shown in Figure 5. In between the letters A and B, C and D, E and F, G and H, I and J, the propeller was measured twenty times each.

The data obtained from the measurements at the five spanwise locations were then used to find the geometric angle of attack, the chord length, and the normalized camber curve. Using linear regression, a polynomial fit was created to find the functional fit of the camber curve. In order for the functional fit of the camber to be more accurate, the camber was broken up into two sections. The first section of the camber was near the leading edge and then the second section of the camber was near the trailing edge.

The chord length was found by finding the distance between the leading edge and the trailing edge. The geometric angle of attack was found by calculating the angle of the line between the leading edge and the trailing edge and the plane in which the propeller rotates. Figure 6 shows the results of one of the normalized spanwise airfoils. It also includes the camber of that airfoil. The angle of attack and the chord length for this cross

section were: 0.2133 radians, and the chord is 0.0829 meters. These data were calculated for each of the five different spanwise locations.

2.2 Lifting Line Code Development

By using the functional fit of the camber, the zero lift angle of attack was found using Equation 8 and 9 (Johnson, 1994). The $\frac{dz}{dx}$ in Equation 8 was found by differentiating the polynomial fit of the camber curve. The x axis is the horizontal axis from Figure 6, and the z axis is the vertical axis.

$$\propto_{L=0} = -\frac{1}{pi} * \int_0^{pi} \frac{dz}{dx} * (\cos\emptyset - 1)\, d\emptyset \quad \textbf{(8)}$$

$$x = \left(\frac{c}{2}\right) * (cos\emptyset - 1) \quad \textbf{(9)}$$

The zero lift angle of attack ($\propto_{L=0}$) was found for all five spanwise locations.

When the geometric and zero lift angle of attack are known, then the only variable still unknown in Equation 7 (found in this chapter heading) is the function $\Gamma(y_0)$. Solving for the $\Gamma(y_0)$ function was not a trivial task. The way to solve for the $\Gamma(y_0)$ is to first to assume a form for this function. One viable form for $\Gamma(y_0)$ is a series of sines and cosines. This is an assumption that is made by Anderson (2007). This is an accurate assumption because a Fourier Series can closely approximate any function over a bounded interval, and as the number of terms in the Fourier Series increases, the closer it approximates the actual function. Anderson also transformed the y in Equation 7 to a $\emptyset$. The transformation that he used was y=-b/2*cos($\emptyset$). This changed the limits of integration in Equation 7 from 0 for the lower limit and pi for the upper limit. As will be shown in Equation 16 (with the new limits), the integral has a closed-form solution.

Another vital piece of information needed to solve for the circulation was that the circulation along the propeller was symmetric across the hub.

One additional piece of information needed in solving Equation 7 was the boundary conditions. The boundary conditions for the propeller are that circulation goes to zero at the tips and at the hub. From Equation 10, it can be seen that the circulation will go to zero under two conditions. The first condition is if the velocity is zero, and the second condition is if the velocity of the air going over the top and bottom of an object is the same. In the case of the propeller, the velocity going around either side of the hub was always the same, and therefore, the circulation will go to zero at that point. The reason the circulation went to zero at the tips is because, "there is a pressure equalization from the bottom to the top of the wing… and hence no lift is created at these points" (Anderson, 2007, p. 403).

$$\boldsymbol{\Gamma = -\oint V * ds} \tag{10}$$

A functional form of $\Gamma(y_0)$ is shown in Equation 11. This form was chosen so that the integral could be solved with a closed-form solution. Only sines were used in this form in order to make sure that on either ends of the propeller, the circulation went to zero. Shown below is the generic function of $\Gamma(\emptyset)$.

$$\boldsymbol{\Gamma(\emptyset) = 2 * b * \sum_{n=1}^{N} A_n * \sin(n * \emptyset) \qquad n = 1, 3, 5, \ldots} \tag{11}$$

The derivative of the circulation needed to be identified in order to be put into Equation 7 $\frac{d\Gamma}{\mathrm{dy}}$ is shown below.

$$\boldsymbol{\frac{d\Gamma}{\mathrm{dy}} = \frac{\mathrm{d}\Gamma}{d\emptyset} * \frac{d\emptyset}{dy}} \tag{12}$$

$$\boldsymbol{\frac{d\Gamma}{\mathrm{dy}} = 2 * b * \sum_{n=1}^{N} n * A_n * \cos(n * \emptyset) * \frac{d\emptyset}{dy}} \tag{13}$$

Putting Equation 9 and 11 into Equation 7 gives:

$$\propto(\emptyset_0) = \frac{2*b*\sum_{n=1}^{N} A_n*\sin(n*\emptyset)}{\text{pi}*V_\infty(\emptyset_0)*c(\emptyset_0)} + \propto_{L=0}(\emptyset_0) + \frac{1}{V_{\infty(\emptyset_0)}} * \int_0^{pi} \frac{\sum_{n=1}^{N} A_n*\cos(n*\emptyset)}{\cos(\emptyset)-\cos(\emptyset_0)} * d\emptyset \quad \textbf{(14)}$$

The integral in this Equation has a closed-form solution. This integral was derived in Appendix E of reference 11.

$$\int_0^{pi} \frac{\cos(n*\emptyset)*d\emptyset}{\cos(\emptyset)-\cos(\emptyset_0)} = \frac{pi*\sin(n*\emptyset_0)}{\sin(\emptyset_0)} \quad \textbf{(15)}$$

Using the result of Equation 13, Equation 12 was reduced to:

$$\propto(\emptyset_0) = \frac{2*b}{\text{pi}*V_\infty(\emptyset_0)*c(\emptyset_0)} * \sum_{n=1}^{N} A_n * \sin(n*\emptyset_0) + \propto_{L=0}(\emptyset_0) + \frac{1}{V_{\infty(\emptyset_0)}} * \sum_{n=1}^{N} n * A_n * \frac{\sin(n*\emptyset_0)}{\sin(\emptyset_0)} \quad \textbf{(16)}$$

Equation 14 was evaluated at a given spanwise location; hence, the subscript on $(\emptyset_0)$ was specified.

One additional parameter, the rotational speed, needed to be known in order so solve for the $A_n's$. The rotational speed of the propeller shaft was identified in order to calculate the approaching velocity at each spanwise location V_∞. With the V_∞ known from the rotational speed of the propeller the only unkowns were the A_n's. Using these results, the circulation distribution along the propeller, was calculated. Using Equation 15 and 16, the lift per span and the total lift was calculated, where ρ was the density of the air (Anderson, 2007, p. 409). The total lift for the propeller is also the thrust of the propeller (Anderson, 2007, p. 409).

$$L_{perSpan} = \rho * V_\infty(y_0) * \Gamma(y_0) \quad \textbf{(17)}$$

$$L_{total} = \int_{-b/2}^{b/2} L_{perSpan}(y) * dy \quad \textbf{(18)}$$

Using the above procedure, Figure 3 was generated. This figure shows a circulation distribution along the propeller for a given rotational speed.

It is important to note that the highest location of circulation is a little inboard of the tips, the circulation went to zero at the hub and tips, and the circulation was a smooth curve without any discontinuities or sharp slope changes. One of the correction factors that was made using the Blade Element Theory was the lift near the tips was corrected so that they went to zero. The Blade Element Theory automatically assumes this correction because of the boundary conditions used when it was solved. The lift near the hub, using the lifting line theory, was also different from that estimated by Blade Element Theory. Both theories estimate a zero lift at the hub, but the slope of the lift at the hub is different. The lift calculated using Prandtl's lifting line theory predicted a smooth transition of lift from one location to another and at the hub, the slope is zero. For the Blade Element Theory, the slope of the lift near the hub is a nonzero value. The value of highest circulation was a function of geometry. A different propeller would have similar circulation as the one shown in Figure 7, but the different geometry would make the location of the maximum circulation different.

The thrust analysis for this propeller can be performed for any rotational speed. The rotational speeds were chosen to match up with the speeds from the tests that were run.

Figure 4: The apparatus used to find the propeller geometry

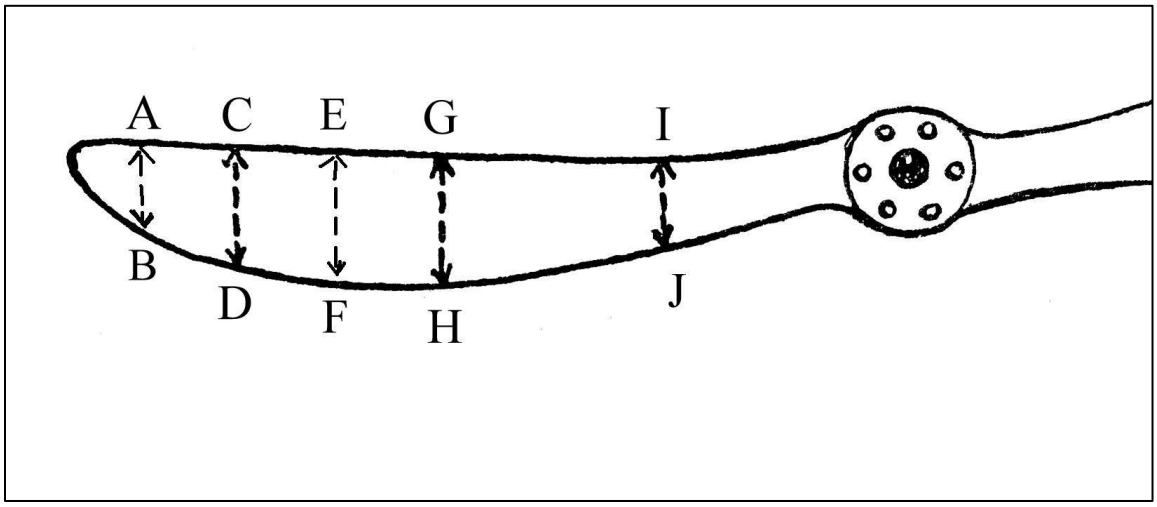

Figure 5: Measurement of five spanwise locations

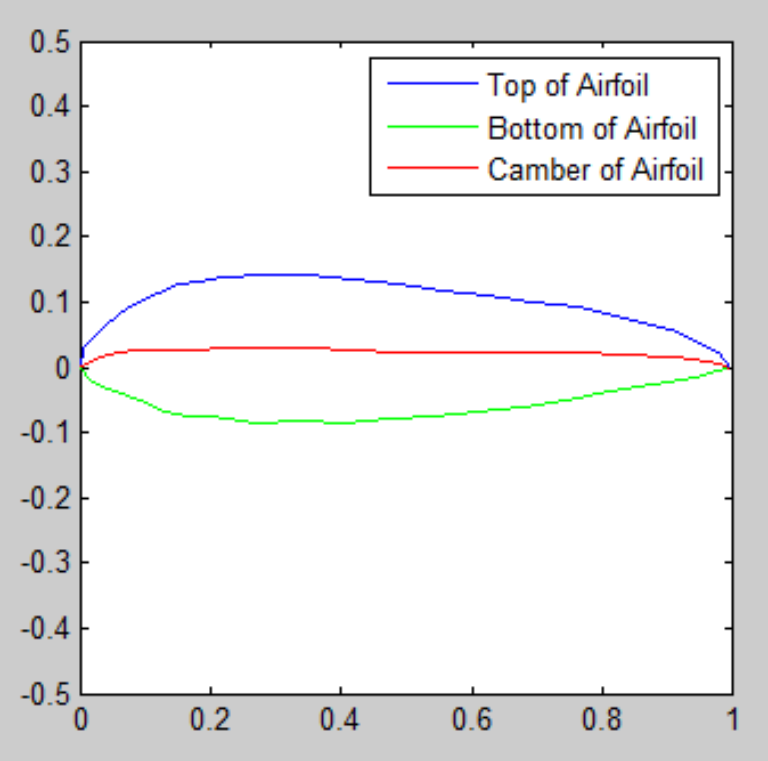

Figure 6: Normalized airfoil at one spanwise location of the propeller.

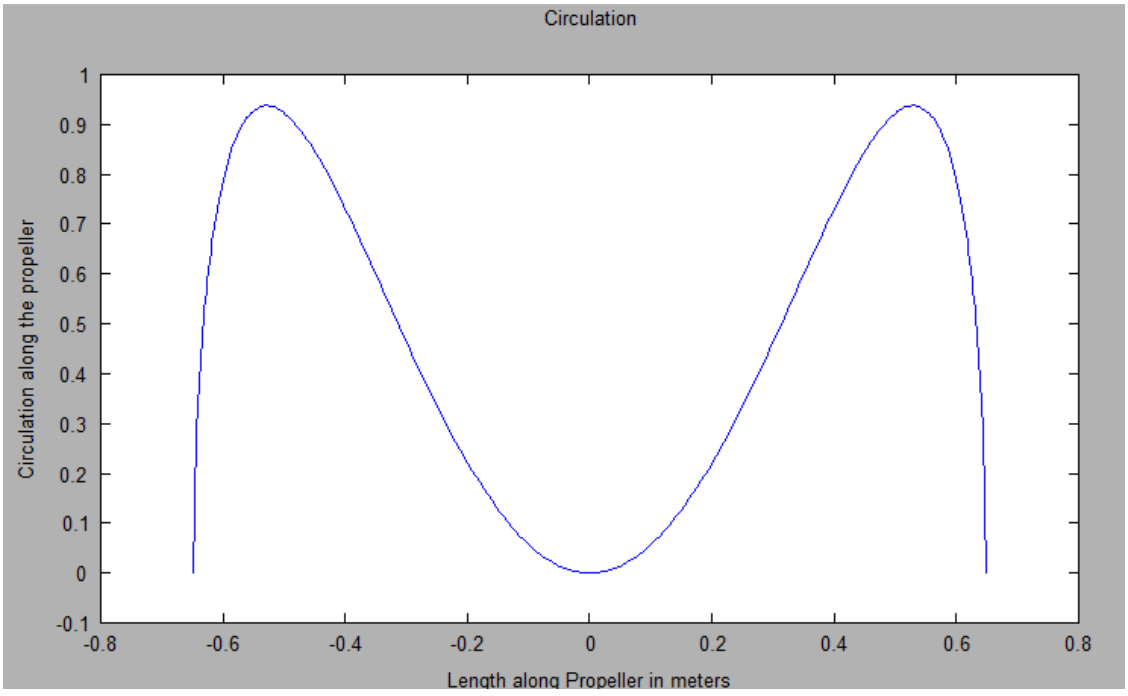

Figure 7: The lift per unit span of a propeller.

CHAPTER 4

EXPERIMENTAL SETUP AND PROCEDURE

In order to measure the thrust of the propeller at different speeds, a testing rig and a data acquisition system were designed and built. Figure 8 shows the test rig set up right before some of the tests.

The test rig consisted of: a frame that held the components together, an engine, a drive shaft that had linkage between the engine and propeller shaft, a speed and a thrust sensor. Figure 9 is a sketch of how the different components were assembled and how they operated together.

The frame had three wheels on it, two in the back and one on the front. The wheels were on slightly inclined ramps. The inclined ramps served two purposes. The first was to give the wheels a smooth surface on which to roll. When the thrust was produced by the propeller, the frame would move forward a few inches, so the ramps needed to allow forward movement. The second purpose of the inclined ramps was to compensate for a slanted driveway (where the tests were performed) to make sure the test rig did not roll backwards. The added forward force from the inclined ramp was accounted for when the thrust from the propeller was calculated.

One side of the thrust sensor was connected by a rope to the test rig. The other side was anchored to the ground. The thrust from the propeller was directed through the frame through the rope and through the thrust sensor. This is very important because the

thrust produced by the propeller was directed through the thrust sensor. There was a small amount of friction from the wheels that countered the thrust of the propeller that produced an inaccuracy in the thrust measurement.

Behind the propeller was approximately 100 feet of unobstructed space. This orientation was chosen because an obstruction close to the propeller could affect the airflow and hence the performance of the propeller.

3.1 Speed Sensor

The speed sensor on the test fixture was made by connecting a disk to the propeller shaft. The disk had one hole in it. On one side of the disk was an Infrared LED, and on the other side was an Infrared Diode. When the propeller shaft would spin around there was only one position in the rotation where the phototransistor would ‘see’ the IR light; see Figure 10. This was converted to an electrical signal. See Figure 11 for the electrical schematic of the speed sensor.

To minimize the effects of noise, a Schmitt trigger was implemented on the output of the photo diode, and a box was put around the whole system to stop any rays from the environment. One pulse was equated to one time around. The output signal was fed into the Data Acquisition System (DAQ). The DAQ system measured the time it took between pulses. This is then easily converted to rotational speed.

3.2 Thrust Sensor

The thrust sensor consisted of four mechanical arms with a spring arranged in between the arms. When a load was applied on either end of the thrust sensor, the arms would move and make the spring deflect. The higher the load was, the more the

deflection was. At the same time, a potentiometer was connected to the arms so that the amount of load was related to the voltage on the potentiometer. Figure 12 shows a Computer Aided-Design model of the sensor. The potentiometer, which is part of the sensor, was connected to the DAQ system as shown in Figure 13.

Both these sensors were calibrated. The way that the speed sensor was calibrated was by the following. First, a known frequency square wave signal was put on one of the digital input pins. The pulses were counted until another digital input pin read a high signal from the speed sensor, which would then write how many known frequency pulses were captured between the last pulse. This information was then read into a desktop computer to wait postprocessing.

In order to calibrate the thrust sensor, a high-resolution scale was used. The scale had a resolution of 0.1 Newton's. When the engine was off, a load was applied to the test fixture that was parallel to the line of action of the propeller thrust. At different applied forces, both the force and the voltage from the potentiometer were recorded. 39 forces were applied between 0 to 100 Newton's (the thrust from the propeller never exceed 100 Newton's); see Figure 14. This information was used in the postprocessing. The raw value from the potentiometer was read into the Arduino and then into a desktop, and during the postprocessing stage, the calibration data were used. A least square model was used for the calibration data. The R squared value was .9955.

3.3 Running the Test and Data Analysis

Components were set up as described in Figure 10 and tests were performed. A laptop was connected to the DAQ system and it recorded the results from the tests. The process that was followed when a test was performed was the engine was started and the

throttle was adjusted to make the propeller rotate at a certain speeds. Once a certain speed was attained, that speed was maintained for approximately 5 to 10 seconds, then the throttle was adjusted for a different speed. After this, the test was stopped and the data was recorded. This process was followed multiple times and at different speeds. After all the data were collected, postprocessing was performed to find the thrust at different speeds. In the data analysis, the calibration factors were used to change the raw data into either speed with units of rotations per second, or for the thrust sensor units of Newton's.

Figure 8: Test fixture

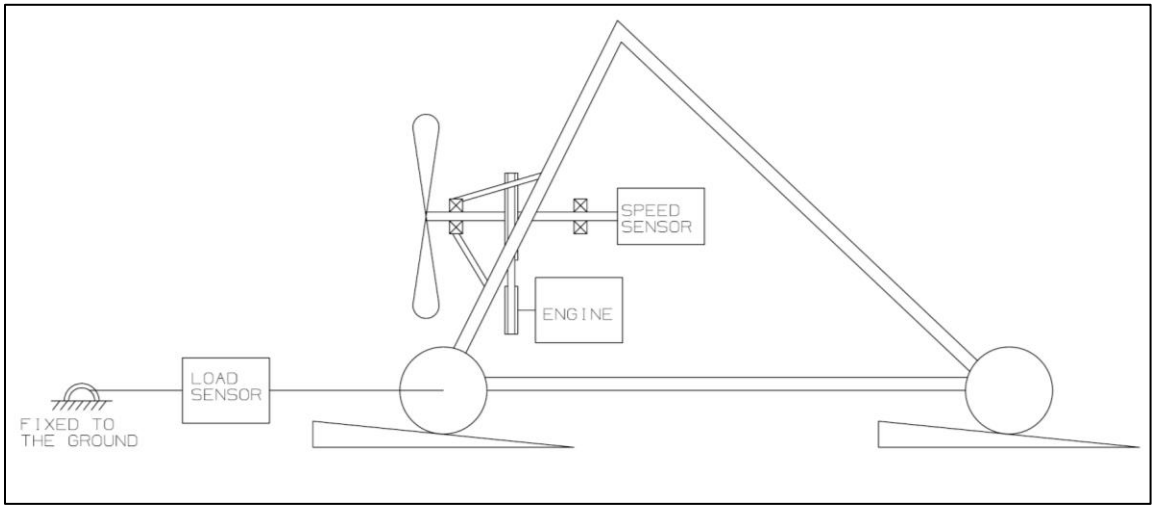

Figure 9: Sketch of the components on the test fixture.

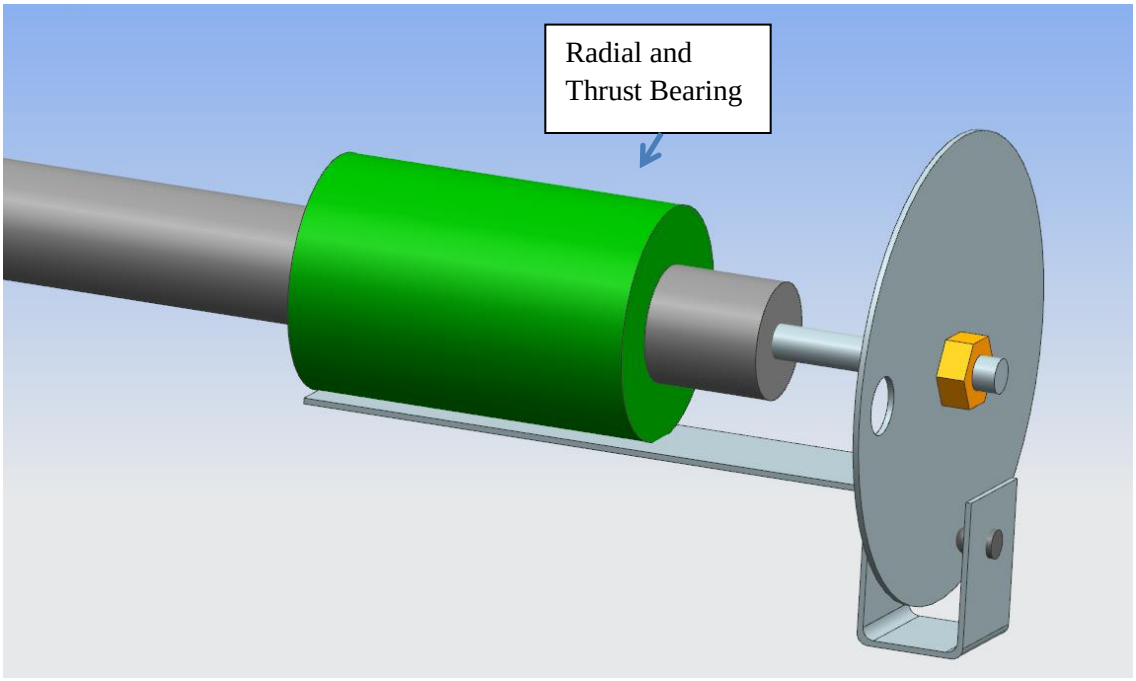

Figure 10: Speed sensor

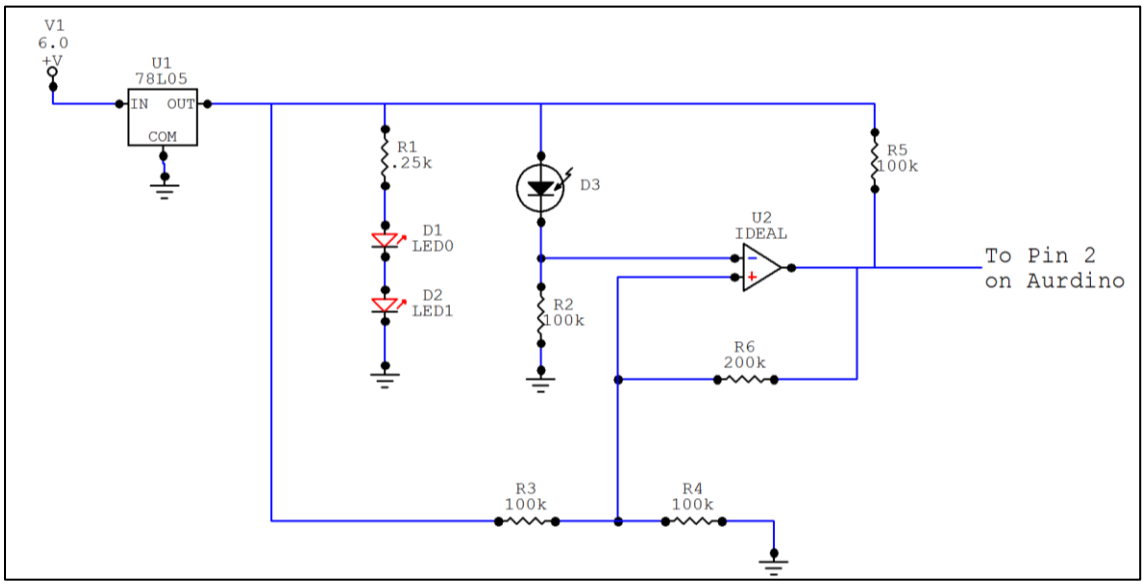

Figure 11: Electrical schematic for the speed sensor

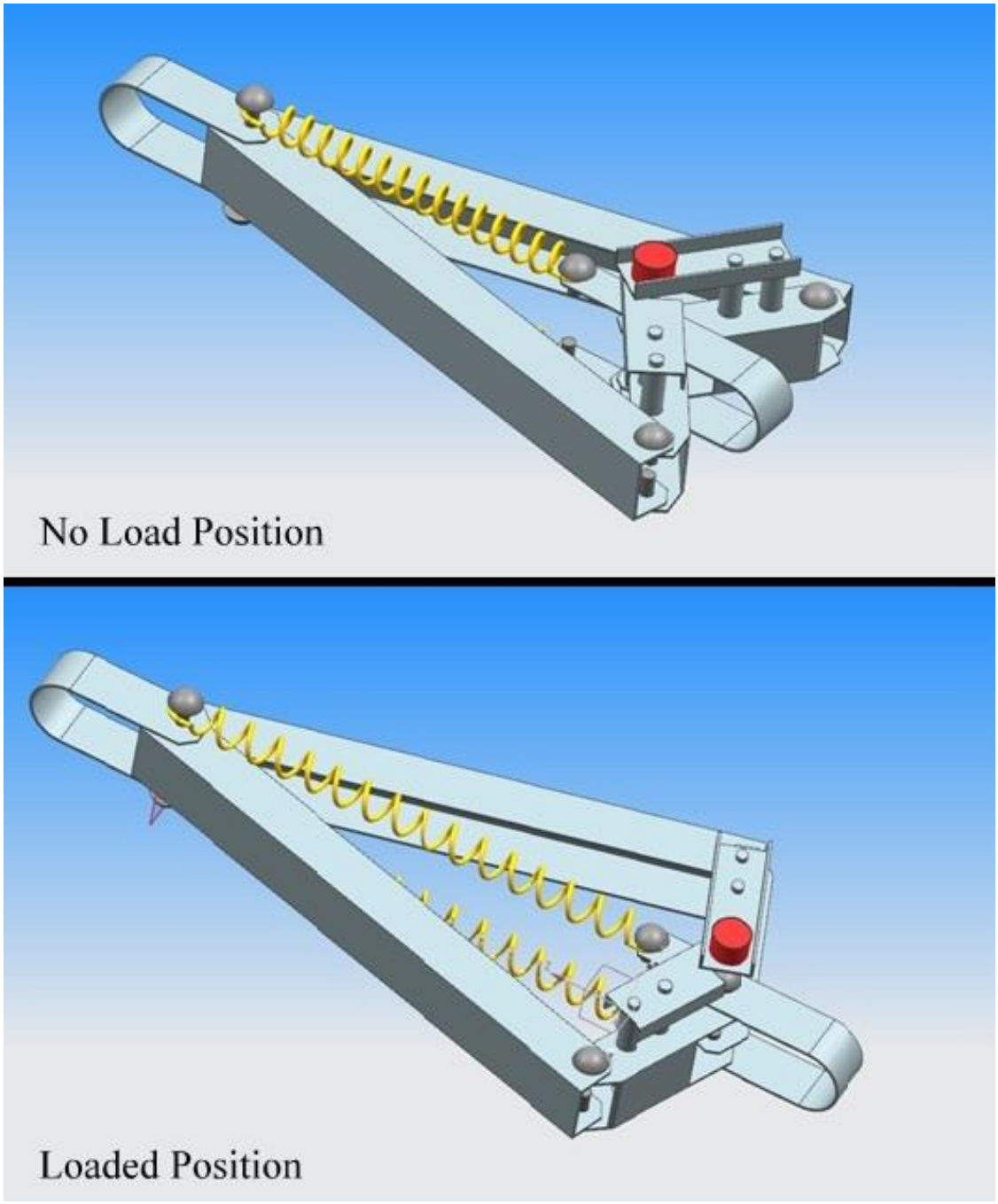

Figure 12: Model of thrust sensor in the retract and extend position.

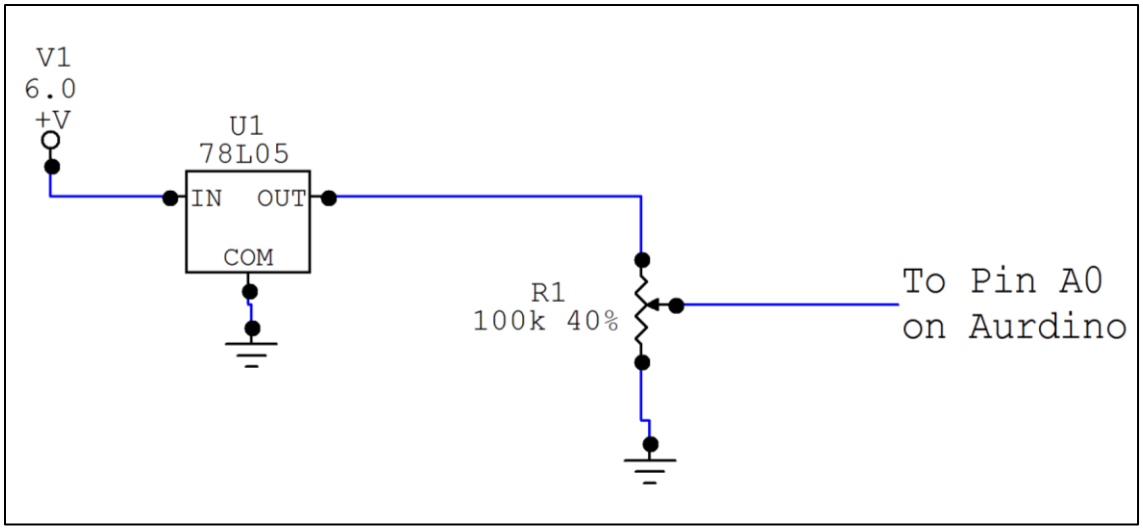

Figure 13: Electrical schematic for the thrust sensor.

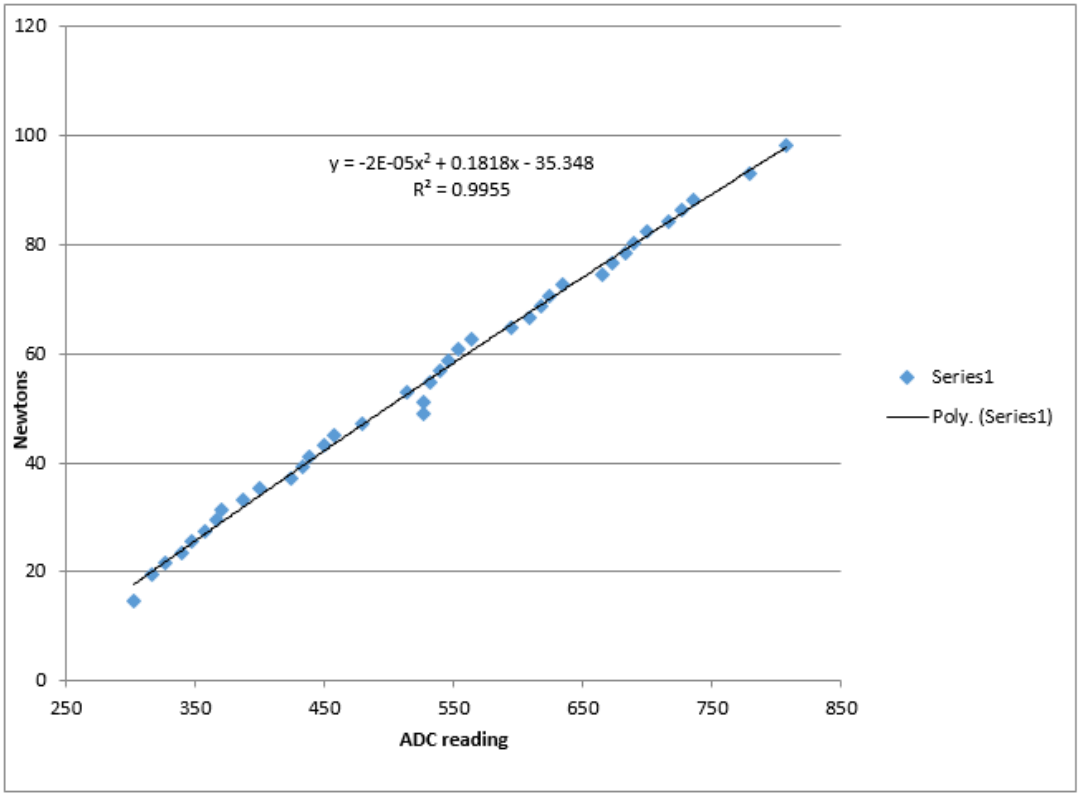

Figure 14: Calibration curve for the thrust sensor

CHAPTER 5

RESULTS AND DISCUSSION

The thrust of the propeller was a function of the rotational speed. The experimental and theoretical results are shown in Figure 15. The theoretical result predicted by Prandtl's lifting line theory and that obtained by Blade Element Theory are shown. Momentum theory was not used in this analysis because the induced velocity is unknown, which is a required parameter in order to use momentum theory. An obvious conclusion that can be made from this plot is that there is an error between the theory and the experimental results. The actual error for each rotational speed is tabulated in Table 1.

4.1 Uncertainties and Error Analysis

In the measurements performed in the tests described, there are some measurement errors that create a certain amount of uncertainty in the results obtained. This section descibes the errors associated with the different measurements. The three main measurements were: the measurement of thrust from the thrust sensor, the measurement of speed from the speed sensor, and the angle of attack of the propeller geometry.

4.1.1 Thrust Sensor Uncertainty

There are a few major sources of errors in the thrust measurements. The thrust sensor was calibrated against a scale that had a resolution of 0.1 Newton's, and because of electronic noise, the voltage reading from the data oscillates about 2 bits or approximately 0.03 Newton's. In addition, because of how the thrust sensor was situated in the test setup, there will be a small amount of frictional force from the wheels that the thrust sensor will not see. This frictional force, though unknown exactly, will be dependent on the rolling coefficient. The coefficient for a bicycle tire is around .0055. This value times the normal force gives the frictional force of 3.5 Newton's, which is another factor in the uncertainty of the thrust measurements. There are a few other minor sources of error that are negligible compared to these other errors. When all these are combined, the error in the thrust measurement could be as high as 3.7 Newton's.

4.1.2 Speed Sensor Uncertainty

The speed sensor counts the pulses between every rotation. These pulses are integer numbers so associated with them are round off errors. For example, if on average there are 24.5 pulses every revolution, then the sensor will read 24 pulses for the first revolution and 25 for the next. By just looking at the pulses for one rotation, the rotational speed could have a lot of error, but if multiple rotations are averaged, then the rotational speed is very accurate. The postprocessing code used an average rotational speed to minimize the error.

4.1.3 Angle of Attack Uncertainty

When the geometry of the propeller was measured, there was associated error. To measure the angle of attack, the top and bottom surfaces were measured with a tape measure (for the x direction) and a digital caliper (for the z direction), and then the angle of attack was found from these data. The error with a tape measure is about 60 thousands of an inch, and with a caliper, 1 thousands of an inch. By doing the calculations for the propeller tip, this correlates to an angle of attack error of .25 degrees. At other spanwise locations the angle of attack error will be less.

4.2 Discussion

One source of error was an assumption made in the theoretical calculation. In the calculation, the velocity vector of the incoming air was assumed to only be in the same plane as the rotation of the propeller blade. In reality, there was a small component of the incoming velocity vector that was perpendicular to the plane of rotation. I will call this velocity component the perpendicular velocity. The effect of the perpendicular velocity vector caused the effective angle of attack to be smaller. This was described in terms of the induced velocity in the literature review, but the same principles apply if the perpendicular components of the velocity are induced or come from the freestream velocity vector. Because there was a perpendicular velocity component all along the propeller, the effective angle of attack along the blade was decreased. The amount of thrust produced by a section of the wing was proportional to velocity of the incoming air and the effective angle of attack. This resulted in each section of the propeller not having as much lift because the effective angle of attack was decreased. Each section had less

lift, so the integral over the whole propeller had less total thrust. This made the calculated thrust closer to the thrust that was measured.

During the test, the perpendicular velocity was not measured, but from the momentum theory in the literature review, it can be calculated. When this velocity component is calculated, there are errors associated with it that come from the assumptions used to develop the momentum theory. To use the momentum theory, the far upstream velocity (V) was set to 0. The thrust calculated from the code was also put into Equation 1, which then calculated the perpendicular velocity. The perpendicular velocity was then put back into the code, which calculated a new thrust. This then became an iterative process of solving the thrust and perpendicular velocity until the solution converged. When a rotational speed of 27 rot/sec (170 rad/sec) was used in the code, the theoretical thrust went from 61.0 Newton's for no perpendicular velocity used to 31.2 Newton's with the perpendicular velocity predicted by momentum theory. This would explain part of the error from Figure 15.

Another explanation why the theoretical and experimental did not match up is from the measurement errors associated with the thrust sensor. From section 4.2.1, there is a possible 3.7 Newton's of constant error between the two. By looking at the error in the angle, the deviation in the thrust can be calculated. For the same rotational of 27 rot/sec with a .25 degree lower angle of attack, the thrust was lowered to 60.9 Newton's, only a .2 Newton difference, which is negligible compared to the other errors. Even if the propeller was vibrating so that the Angle of attack was changed one degree, the difference would only be .8 Newton's.

Prandtl's lifting line assumed a smooth incoming flow. As the air traveled around the blade, trailing edge vortices and wing tip vortices were created. These vortices were present when the following propeller blade approached. The air was not smooth anymore because of the vortices created by the previous blade. The vortices were carried downstream but still impacted the initial conditions of the incoming blade. These vortices took energy from the system and decreased the efficiency of the propeller. The decrease in efficiency was shown by the lower thrust produced for a given rotational speed. If these disturbances to the incoming flow were accounted for in the calculations, then the thrust predicted would be closer to the thrust measured in the experiment.

The last three errors just discussed explain the initial offset in the theoretical vs. experimental plot. But these errors did not explain why there is a dip in the lift at higher speeds. In order to understand this phenomena, the assumptions in the theory need to inspected.

An assumption that was made in developing the equations for the thrust of the propeller was that the flow is a inviscid flow. In reality, when the Reynolds number became too high, the flow went turbulent. The effect caused a decrease in lift, as was shown in Figure 15. However, by using the equations developed, the flow was assumed to never go turbulent, and hence, no decrease in lift was predicted at higher rotational speeds. This explained why the theoretical plot always had a positive slope. On the other hand, the experimental plot had a dip in it. Where the plot started to dip, there was flow separation. Flow separation can happen at high speeds, or higher angles of attack, and sometimes in both instances. The effect of flow separation was that the thrust from the propeller decreased. This is known as stall.

Other assumptions were made in developing the equations. First, there was no friction from the viscosity of the fluid. Secondly, there was an incompressible flow. The first assumption is accurate because at the higher speeds, and the low viscosity, most of the forces will came from the pressure distribution on the propeller blade. A small drag force was developed from skin friction; however, this value was small in comparison to the forces from the pressure distribution on the airfoil. This can be quantified by looking at the Reynolds number, which is a ratio of the momentum forces divided by the viscous forces. Another way to look at this ratio is the ratio of the forces contributed by the pressure distribution over the propeller divided by the forces from the viscosity of the fluid. The average Reynolds number is the incoming velocity times the chord length times the density all divided by the dynamic viscosity of the fluid. This is shown in Equation 19:

$$\boldsymbol{Re = \frac{V_{\infty} * \rho * c}{\mu}} \qquad \textbf{(19)}$$

For the propeller at the quickest speed during the test, the Reynolds number was 9.04e5. When the Reynolds number is approximately 5000, the momentum starts to dominate, and the Reynolds number calculated is 180 times above this value.

The assumption that the flow is incompressible is valid and will only deviate by a few percent if the fastest velocity of the propeller is less than 300 mi/hr. (134 m/s) (Anderson, 2007). Just before stall, the tip velocity was 120 m/s. At the higher speeds, the compressibility effects started to be manifested. This accounts for some of the errors at the high speeds.

The overall effectiveness of Prandtl's lifting line theory in predicting the actual thrust was dependent on the rotational speed. When the speed was close to the stall point

of the propeller, but not over it, the error was the least with only a 36% error. The percent error was greater at lower and faster speeds. The errors in the plot for the lower speed were probably due to the errors in the measurements, the decreased effective angle of attack of the propeller, and the disturbances in the incoming flow. At higher speeds, not only did these previous reasons contribute to the error, but also flow separation and compressible flow made more errors in the results.

It was found that by using a Fourier Series to approximate the circulation along the propeller, under certain conditions, the solution became unstable. These instabilities were caused when a lot of spanwise locations were used in the lifting line code. The instabilities were obvious when they happened because the circulation distribution became very erratic. The instability was probably because when there were a lot of spanwise locations to solve for, the frequencies that were used in the Fourier Series became high. To ensure that the solution was stable, the number of spanwise locations had to be limited. When only five spanwise locations were used, the solution showed no signs of instability. To verify this, the code was run when one of the spanwise locations was omitted. The lift that was calculated was within 1% of what the lift was when all the spanwise locations were included. However, for this test, the Fourier Series were sufficient to provide an accurate and stable result; a limitation will occur when a lot of spanwise locations are used.

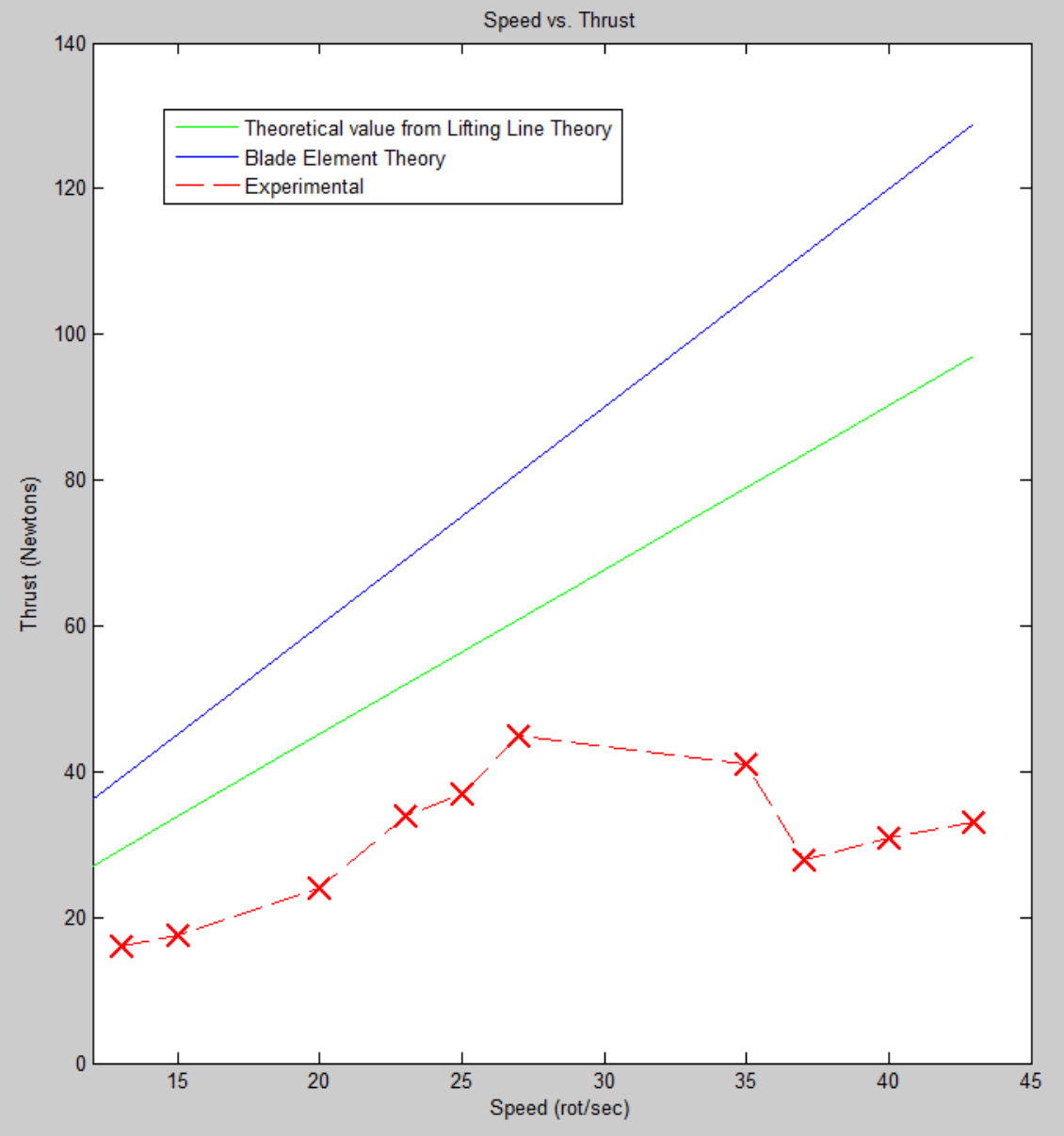

Figure 15: A graph relating the thrust vs. the speed.

Table 1: The percent error between the experimental and theoretical thrust predicted by Prandlt's lifting line theory.

Speed (rot/sec)	$Error\% = \frac{abs(Thrust_{actual} - Thrust_{theretical})}{Thrust_{actual}}$
13	84%
15	94%
20	89%
23	53%
25	53%
27	36%
35	93%
37	199%
40	192%
43	195%

CHAPTER 6

CONCLUSION

An experiment was carried out to find the thrust of a propeller at different rotational speeds. By using a modified version of Prandtl's classical lifting line theory, the thrust of a propeller was calculated at these same speeds. By comparing the results, it was found that the theory over predicted the experimental thrust. When the rotational speed did not cause the propeller to stall, the error was between 84% at low speeds to 36% close to the stalling point of the propeller. At speeds above the stall point, the error increased tremendously up to 195% and from the data trend, it looked like it would continue to increase at even higher speeds.

These errors are likely associated with a few factors. For all speeds, there are three big factors. They are the measurement errors from the thrust sensor, neglecting the velocity component perpendicular to the plane in which the propeller rotates, and the non-uniform flow in which the propeller blade constantly moves. For medium speeds, the error is due to flow separation, which is manifested by a rapid decrease in lift. The theory never took this into account. For high speeds only, another error shows up. This additional error is due to compressible flow, which again the theory did not take into account.

Prandtl's lifting line theory applied to propellers gives a reasonably result as long as the propeller does not stall. The reasonable result still has error associated with it that comes from the assumptions made when the theory was developed.

CHAPTER 7

FUTURE WORK

The measured value was always lower than the calculated value. This means that there are some turbulent and viscous effects that negatively affect the thrust of the propeller. By using a correcting factor, a closer result can be found for the thrust. Some parts of the geometry that should be considered in the correcting factor are the thickness of the airfoils and the 'roundness' of the tips of the airfoil. Another correction factor can be used for high speeds. The lifting line theory assumes incompressible effects, but at high speeds, the tips of the propeller are the first place that compressibility needs to be considered.

A limitation was found in using the Fourier Series. The solution showed signs of instability when a lot of spanwise locations were used. These instabilities might be alleviated if the spanwise locations were chosen in such a way that the different frequencies used in the Fourier Series would not cause the solution to become unstable. This might mean choosing the spanwise locations at certain distances from the hub depending on the number of terms used. Another approach is to use a different type of function besides trig functions to describe the circulation along the propeller blade.

REFERENCES

Anderson, John D. *Fundamentals of Aerodynamics*. Boston: McGraw Hill (2007)

Goldstein, Sydney. "On the Vortex Theory of Screw Propellers." *Proceedings of The Royal Society Mathematical, Physical, & Engineering Sciences*. no. 123 (1929): 440-465. rspa.royalsocietypublishing.org (accessed January 18, 2014).

Gómez-Iradi, S., R. Steijl, and G. N. Barakos. 2009. "Development and Validation of a CFD Technique for the Aerodynamic Analysis of HAWT." *Journal Of Solar Energy Engineering* 131, no. 3: 9. *Academic Search Premier*, EBSCO*host* (accessed January 25, 2014).

Karamcheti, K.: *principles of Ideal Fluid Aerodynamics*, John Wiley & sons, Inc., New York (1966)

Kerwin, Justin E., Massachusetts Institute of Technology, "13.04 Lecture Notes Hydrofoils and Propellers." Last modified 01 2001. Accessed March 14, 2014. http://ocw.mit.edu/courses/mechanical-engineering/2-23-hydrofoils-and-propellers-spring-2007/course-notes/kerwin_notes.pdf.

Johnson, Wayne. *Helicopter Theory*. New York: Dover Publications, inc., (1994).

Rashahmadi, Samrand, Morteza Abbaszadeh, Sana Hoseyni, and Raziyeh Alizadeh. "Design of a Constant Chord Single-Rotating Propeller using Lock and Goldstein Techniques." *World Academy Of Science, Engineering & Technology* 80, 1582-1586. (2011).

Rwigema., M. K. 27th International Congress of the Aeronautical Sciences, "Propeller Bade Element Momentum Theory with vortex wake deflection." Last modified 2010. Accessed March 14, 2014. http://www.icas.org/ICAS_ARCHIVE/ICAS2010/PAPERS/434.PDF.

Sayed, Mohamed A., Hamdy A. Kandil, and El-Sayed I. Morgan. "Computational fluid dynamics study of wind turbine blade profiles at low Reynolds numbers for various angles of attack." *AIP Conference Proceedings* 1440, no. 1: 467-479. *Academic Search (*2012)

Stepniewski, W.z., and C.N. Keys. *Rotary-Wing Aerodynamics*. New York: Dover Publications, inc., (1984)